IEEE Access
Multidisciplinary | Rapid Review | Open Access Journal

Received January 30, 2019, accepted February 20, 2019, date of publication February 27, 2019, date of current version March 25, 2019.

Digital Object Identifier 10.1109/ACCESS.2019.2901983

A HTS-Excitation Modular Flux-Switching Linear Machine With Static Seals

WENZHONG MA, XIAOYANG WANG, YUBIN WANG, AND XIANGLIN LI

College of Information and Control Engineering, China University of Petroleum (East China), Qingdao 266580, China

Corresponding author: Xianglin Li (xianglinli@upc.edu.cn)

This work was supported in part by the National Natural Science Foundation of China under Project 51877215 and Project 51777216, in part by the Application Fundamental Research Funds of Qingdao under Project 17-1-1-28-jch, and in part by the Natural Science Foundation of Shandong Province under Grant ZR2018MEE040.

ABSTRACT This paper proposes and analyzes a novel high-temperature superconducting (HTS) modular flux-switching linear machine for long-stator applications, which adopts the stator with a low-cost salient-pole iron core and accommodates both the armature windings and HTS-excitation windings on the short mover, thus facilitating static seals of cooling Dewar for the HTS windings. The key of the proposed machine is to employ a modular mover structure composed of separate phase modules to achieve a complementary pattern, such that the cogging force can be significantly offset to effectively reduce the force ripple while offering the advantages of very symmetrical back electromotive force (EMF) and high fault tolerance. The operation principle and optimization analysis of the proposed machine with concern on the HTS-excitation characteristics are carried out. Also, by using the two-dimensional finite element method, the electromagnetic performances of the proposed machine are investigated to verify its validity. The results show that it can offer symmetrical and sinusoidal back-EMF, high fault tolerance, and low force ripple.

INDEX TERMS Finite element method (FEM), flux-switching machine, high-temperature superconducting excitation; linear machine.

I. INTRODUCTION

For the linear motion applications such as urban rail transit, the linear machines can provide a direct thrust force without the energy conversion from rotary to linear motion compared to the rotary machines [1], [2]. It is known that the linear permanent-magnet synchronous (LPMS) machine has higher power density and efficiency than the linear induction machines [3]. However, for linear long-stator applications, the conventional LPMS machine inevitably suffers a significant cost since a large number of magnets or armature windings need to be set along the long stator. To solve this issue, a series of primary PM linear machines [4]–[7] have been presented and attracted much attention, which places both the magnets and armature windings on the short mover and adopts the long stator with low-cost salient-pole iron core. Moreover, in order to improve the disadvantages of asymmetric magnetic circuit and large cogging force, the modular and complementary structures have been investigated and applied for the primary PM linear machines [8]. However, when these existing primary PM linear machines are used for the high-power direct-drive applications, they still face bulky volume and reduced power density.

In recent years, the high-temperature superconducting (HTS) machines have attracted increasing attention in high-power direct-drive applications [9], [10], because it is easy for the HTS machines to achieve large power capacity, high power density and efficiency [11]–[13]. Also, since the air-gap magnetic field can be flexibly regulated by controlling the HTS-excitation current, the HTS machine can easily achieve the high-speed constant-power operation [14]. In general, compared with the rotor HTS-excitation machine using rotating dynamic seals of cryogenic transfer coupling and cooling Dewar [15], the stator HTS-excitation machine with static seals has a simple refrigeration system design, thus greatly reducing the structural complexity and manufacturing costs [16], [17]. Recently, a rotary 12-slots/14-poles stator HTS-excitation flux switching (HTS-FS) machine with static seals as shown in Fig. 1(a) was proposed, and its operation principle and electromagnetic performances were also investigated in [18].

Based on the configuration of the presented rotary 12-slots/14-poles stator HTS-FS machine, a 12-slots/14-poles HTS flux-switching linear (HTS-FSL) machine can be

The associate editor coordinating the review of this manuscript and approving it for publication was Mehmet Alper Uslu.

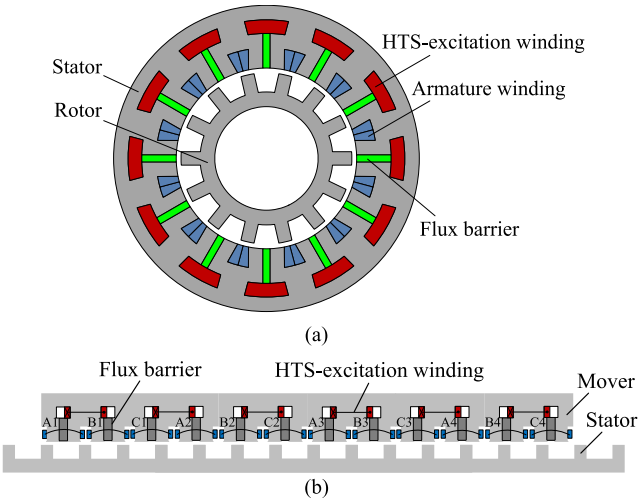

FIGURE 1. Topologies of the 12-slots/14-poles HTS-FS machine. (a) Rotation type. (b) Linear type.

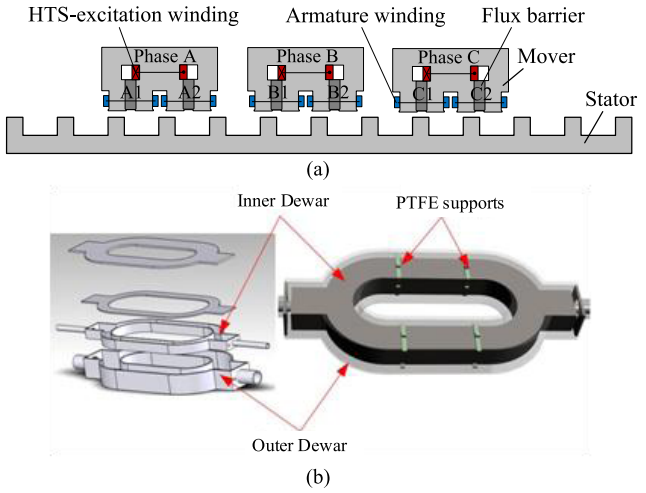

FIGURE 2. Configuration of the proposed HTS-MFSL machine. (a) Cross section. (b) Dewar assembly.

directly obtained by splitting it along the radial direction and unrolling it as shown in Fig. 1(b). However, this kind of HTS-FSL machine exists the problems of asymmetrical magnetic circuit, large cogging force and phase magnetic circuit coupling. Therefore, this paper is to derive and analyze a HTS-excitation modular flux-switching linear (HTS-MFSL) machine for long-stator applications, in which the modular mover design can significantly reduce the cogging force and improve the fault tolerance, meanwhile it is easy to implement static seals of cooling Dewar for the HTS windings accommodated on the short mover. The configuration and operating principle of the proposed HTS-MFSL machine will be described in Section II. Section III will focus on investigating its design rules and analyzing the influence of key design parameters on its electromagnetic characteristics. Then, in Section IV, its electromagnetic performance analysis will be conducted by using two-dimensional finite element method (2D-FEM). Finally, some conclusions will be drawn in Section V.

II. CONFIGURATION AND OPERATION PRINCIPLE

A. CONFIGURATION

Fig. 2(a) shows the configuration of the proposed HTS-MFSL machine. The key design is to adopt the separate modular mover structure, in which each phase module spans λ_1 apart:

$$\lambda_1 = \left(k - \frac{1}{m}\right)\tau_s \tag{1}$$

where k is a positive integer ($k = 3, 4, 5\ldots$), m is the number of phases, and τ_s is the stator pole pitch. That is, for the presented 3-phase HTS-MFSL machine as shown in Fig. 2(a), the position of three phase modules are mutually 120° electrical degrees apart. For each phase module, there are two cavities set on the mover yoke with only one HTS-excitation coil as single layer winding placed inside, thus it is easy to implement simple refrigeration system design and static seals of cooling Dewar. As shown in Fig. 2(b), a special double-layer Dewar is designed to accommodate each HTS-excitation coil for its cooling. That is, the racetrack inner Dewar is suspended within an outer Dewar by using the poly tetra fluoroethylene (PTFE) supports, and the HTS-excitation coil is housed in the inner Dewar. The gap between the inner Dewar and the outer Dewar is evacuated to achieve excellent thermal insulation. Thus, the cryogenic liquid nitrogen flows in the inner Dewar to immerse the HTS-excitation coil to keep its working temperature, and the magnetomotive force (MMF) direction of each HTS-excitation coil is designed the same.

Moreover, there are two mover teeth on each phase module, and armature windings are wound around each mover tooth in which a flux barrier is inserted. The modular mover structure can offer several advantages: (i) reducing cogging force due to complementary pattern; (ii) improving the fault tolerance due to independent phase magnetic circuit; (iii) facilitating batch processing to save costs. In addition, the proposed HTS-MFSL machine retains a simple salient-pole stator structure consisting of low-cost iron, which is very suitable for long-stator applications.

B. OPERATION PRINCIPLE

In the proposed HTS-MFSL machine, each phase armature winding consists of two coils. For example, the Coil A1 and Coil A2 are connected in series to form the Phase A winding. As shown in Fig. 3, the maximum value of Phase A flux-linkage can be achieved at two special mover positions. At the Position 1 as shown in Fig. 3(a), the main flux excited by the HTS-excitation coil mainly go through the mover yoke, stator iron, air-gap, and left halves of the teeth of Coil A1 and Coil A2. According to the principle of minimum magnetic resistance, it can be assumed that the flux linkage of Coil A1 reaches the negative maximum value, while the flux linkage of Coil A2 reaches the positive maximum value. If the Position 1 is termed as the initial position with $\theta_e = 0°$, when the mover moves 1/2 stator pole pitch to the Position 2, namely $\theta_e = 180°$ as shown in Fig. 3(b), the flux linkages

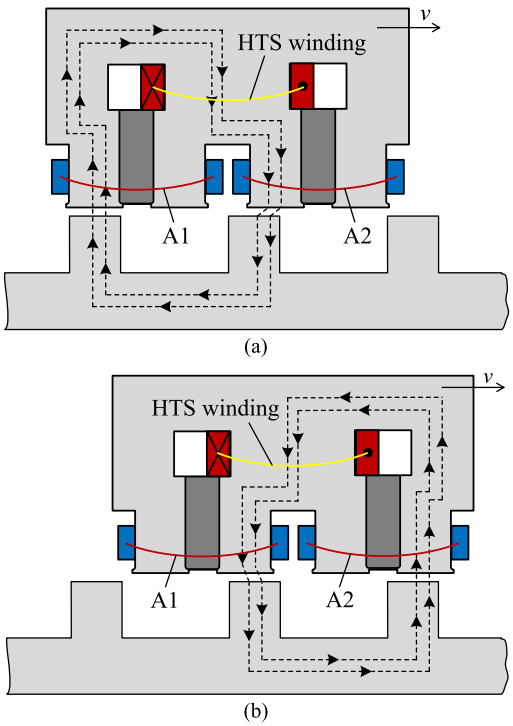

FIGURE 3. Operating principle schematic of the proposed machine. (a) Position 1, $\theta_e = 0°$. (b) Position 2, $\theta_e = 180°$.

of Coil A1 and Coil A2 will reach the positive and negative maximum values, respectively. Hence, it can be found that the flux linkages of Coil A1 and Coil A2 are bipolar, but there is a 180° phase difference between them, thus connecting in reverse series.

To validate the operation principle analysis, by using the 2D-FEM, the no-load flux distributions of Phase A with different mover positions, namely, $\theta_e = 0°, 90°, 180°, 270°$, respectively, are also plotted in Fig. 4. It can be observed that the FEM results well agree with the theoretical analysis. As the mover moves by one stator pole pitch, the flux linkage of each phase can change in one electrical period, thus causing the alternating electromotive force (EMF).

III. INFLUENCE OF KEY DESIGN PARAMETERS ON ELECTROMAGNETIC PERFORMACES

A. GEOMETRY DESIGN CONSTRAINTS

In order to obtain an optimal performance, it is necessary to investigate the influence of key design parameters on the machine electromagnetic characteristics [19], [20]. The dimensional parameters of the proposed HTS-MFSL machine are defined as shown in Fig. 5. In order to ensure successful flux switching and maximize the phase flux-linkage, the initial geometry design of the mover and stator are constrained by the conditions below:

$$\begin{cases} w_{mt} \approx w_{st} \approx h_{my} \approx h_{sy} \\ \tau_s \approx \tau_m \\ w_{mt} < w_{ht} \end{cases} \quad (2)$$

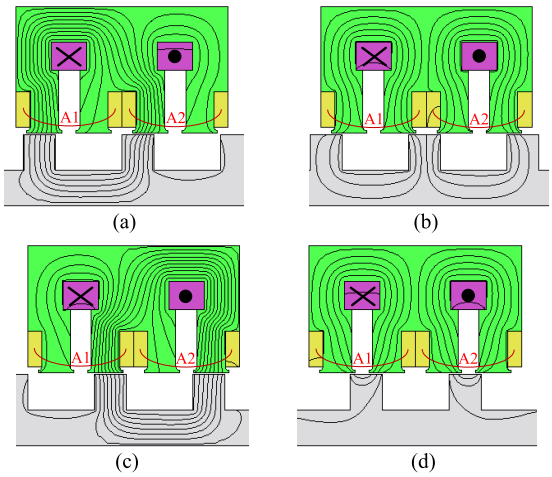

FIGURE 4. No-load flux distribution of Phase A in the proposed machine. (a) $\theta_e = 0°$. (b) $\theta_e = 90°$. (c) $\theta_e = 180°$. (d) $\theta_e = 270°$.

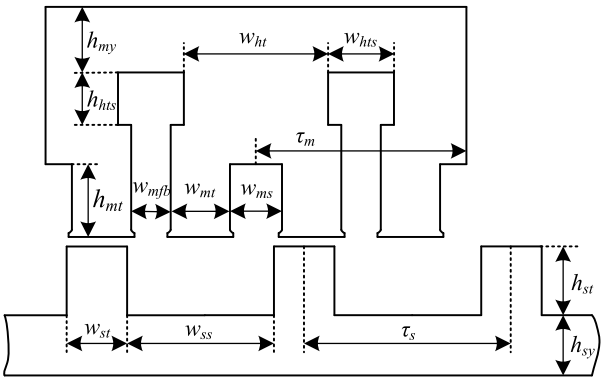

FIGURE 5. Determination of dimensional parameters of the proposed machine.

where w_{mt}, w_{st} and w_{ht} are the mover tooth width, the stator tooth width, and the HTS-excitation tooth width, respectively. h_{sy} and h_{my} are the stator yoke height and the mover yoke height, respectively. τ_m is the mover pole pitch of each phase module, and τ_s is the stator pole pitch.

Based on the initial geometry design constraints, by using the 2D-FEM, the influences of the mover flux barrier width w_{mfb}, the stator pole pitch τ_s, the stator tooth-width coefficient λ_{st} on the electromagnetic characteristics of the proposed HTS-MFSL machine are investigated, in which the performance indicators concerned mainly involve the no-load back-EMF root-mean-square (RMS), thrust force, cogging force and force ripple. The optimization design flow is shown in Fig. 6.

B. FLUX BARRIER WIDTH

First of all, because the mover flux barrier has a significant influence on the flux leakage and the tooth-slot effect, with the aforementioned geometry design constraints, by using the 2D-FEM, the variations of the electromagnetic characteristics of the proposed HTS-MFSL machine with the mover flux

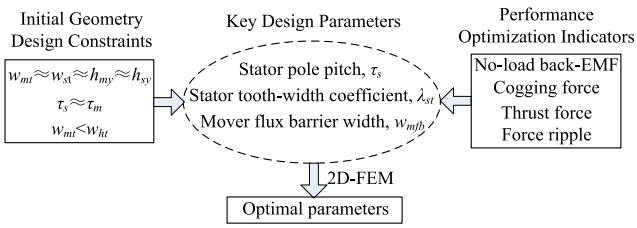

FIGURE 6. Optimization design flow for the proposed machine.

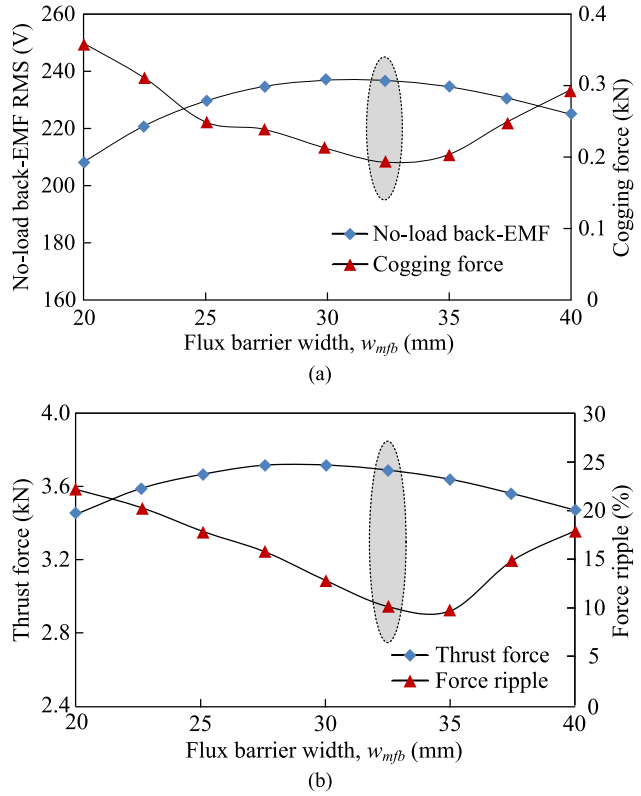

FIGURE 7. Variations of the electromagnetic characteristics with the flux barrier width w_{mfb}. (a) Back-EMF and cogging force. (b) Thrust force and force ripple.

barrier width w_{mfb} in the range of 20 mm to 40 mm are investigated and the results are shown in Fig. 7(a) and 7(b). It can be observed from Fig. 7(a) that when the mover flux barrier width is about 32.5 mm, the minimum cogging force can be reached while keeping a large no-load back-EMF. In this case, the satisfactory thrust force capability and the acceptable force ripple can also be offered as shown in Fig. 7(b).

C. STATOR POLE PITCH

In addition, due to flux switching principle resulting in special magnetic circuit structure, the stator pole pitch as a key parameter has a great effect on the no-load back-EMF waveform. Thus, keeping the stator tooth width constant, by using the 2D-FEM, the variations of the electromagnetic characteristics of the proposed machine with the stator pole pitch τ_s are also investigated as shown in Fig. 8(a) and 8(b).

TABLE 1. Comparison of the THD of the no-load back-EMF waveforms under different stator pole pitch τ_s.

Stator pole pitch, τ_s (mm)	THD of no-load back-EMF waveform (%)
120	12.0
125	10.6
130	9.6
135	9.2
140	12.3
145	18.6
150	18.9

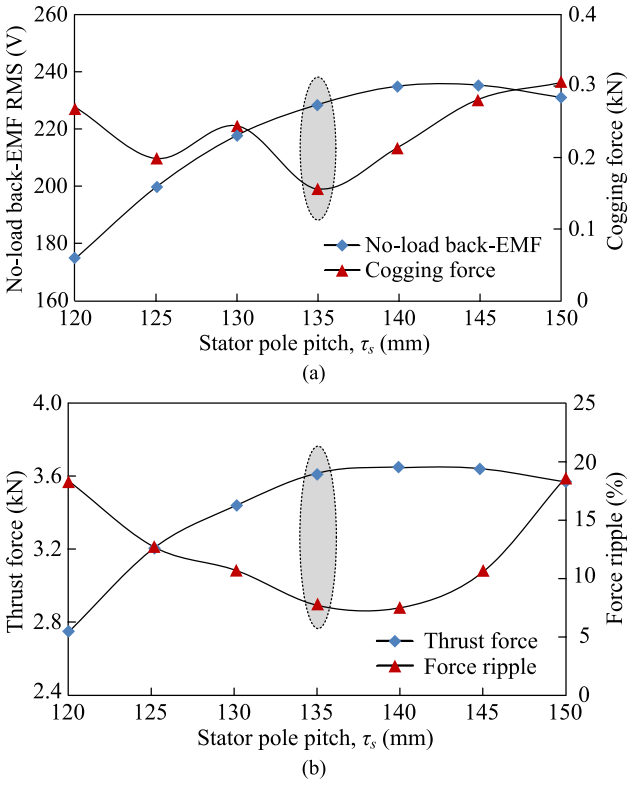

FIGURE 8. Variations of the electromagnetic characteristics with the stator pole pitch τ_s. (a) Back-EMF and cogging force. (b) Thrust force and force ripple.

Meanwhile, the total harmonic distortion (THD) of the corresponding no-load back-EMF waveforms are calculated and comparatively listed in Table 1. It can be found from Table 1 that when the stator pole pitch τ_s is set as 135 mm, the THD of back-EMF waveform reaches the minimum value, thus indicating a very sinusoidal no-load back-EMF.

What is more, from Fig. 8(a), it can be found that the no-load back-EMF gradually increases with the τ_s, but from Fig. 8(b), it can be seen that the variations of the thrust force and force ripple with the stator pole pitch τ_s are obviously opposite, namely, the thrust force increases with τ_s while the force ripple decreases when τ_s is smaller than 135 mm. Meanwhile, the cogging force also reaches around the minimum value when τ_s is set as 135 mm as shown in Fig. 8(a).

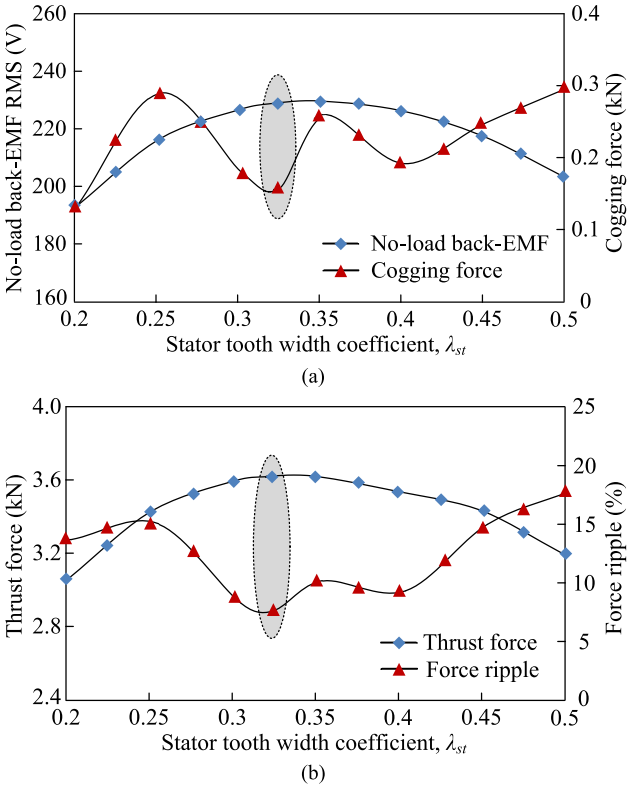

FIGURE 9. Variations of the electromagnetic characteristics with the stator tooth-width coefficient λ_{st}. (a) Back-EMF and cogging force. (b) Thrust force and force ripple.

D. STATOR TOOTH-WIDTH COEFFICIENT

In the proposed HTS-MFSL machine, the stator tooth-width coefficient λ_{st} can be defined as

$$\lambda_{st} = w_{st} / \tau_s \tag{3}$$

Keeping the τ_s constant 135 mm, Fig. 9 (a) and 9(b) show the variations of the electromagnetic characteristics with the stator tooth-width coefficient λ_{st} in the range of 0.2-0.5. When the stator tooth-width coefficient λ_{st} is smaller than 0.325, the back-EMF and thrust force increase with the increase of λ_{st}. However, when the λ_{st} is over 0.325, the back-EMF and thrust force will gradually reduce due to intensified flux leakage. Hence, the stator tooth-width coefficient λ_{st} can be selected as 0.325 for obtaining the optimal back-EMF and thrust force. And in this case, the minimum cogging force and force ripple can also be achieved as depicted in Fig. 9. Meanwhile, the THD of the no-load back-EMF waveforms under different stator tooth-width coefficient are calculated and comparatively listed in Table 2. It can be found that when the stator tooth-width coefficient is set as 0.325, the THD of the no-load back-EMF waveform can further reduce to 7.6%.

E. HTS-EXCITATION MMF

Based on the above structural parameter analysis, and in order to take full advantage of the strong magnetic field capability of the HTS excitation, the HTS-excitation magnetomotive force (MMF) in the proposed HTS-MFSL machine should be carefully designed. As depicted in Fig. 10(a), the variations of the flux densities in the mover tooth and air-gap with the HTS-excitation MMF are investigated, in which the B_{tooth} and the $B_{\text{air-gap}}$ represent the flux densities in the mover tooth and the air-gap, respectively. It can be seen that when the HTS-excitation MMF is less than 5000 At, the B_{tooth} and the $B_{\text{air-gap}}$ increase almost linearly, and then gradually becoming saturated. Therefore, concerned about the influence of the magnetic saturation of iron materials on the flux distribution, the HTS-excitation MMF can be

TABLE 2. Comparison of the THD of the no-load back-EMF waveforms. under different stator tooth-width coefficient λ_{st}.

Stator tooth width coefficient, λ_{st}	THD of no-load back-EMF waveform (%)
0.200	11.09
0.225	9.97
0.250	8.60
0.275	7.85
0.300	7.22
0.325	7.60
0.350	7.63
0.375	8.64
0.400	9.33
0.425	9.81
0.450	10.40
0.475	11.39
0.500	11.53

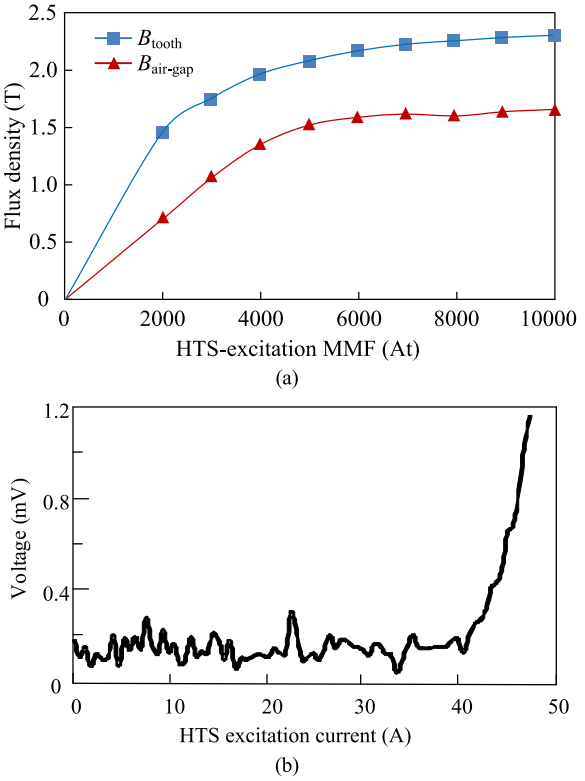

FIGURE 10. HTS-excitation characteristic analysis. (a) Variations of the flux density in the mover tooth and air-gap with the HTS-excitation MMF. (b) Measured I/V characteristics of the fabricated HTS-excitation coil.

TABLE 3. Key design parameters of the proposed HTS-MFSL machine.

Parameters	Value
Mover speed, v (m/s)	6.75
Mover pole pitch, τ_m (mm)	150
Mover tooth width, w_{mt} (mm)	38.75
Mover slot width, w_{ms} (mm)	40
Mover flux barrier width, w_{mfb} (mm)	32.5
HTS-excitation slot width, w_{hts} (mm)	50
HTS-excitation tooth width, w_{ht} (mm)	100
HTS-excitation slot height, h_{hts} (mm)	40
Mover yoke height, h_{my} (mm)	45
Mover tooth height, h_{mt} (mm)	50
Stator pole pitch, τ_s (mm)	135
Stator tooth width, w_{st} (mm)	44
Stator tooth height, h_{st} (mm)	60
Stator yoke height, h_{sy} (mm)	45
Air-gap length, g (mm)	2
Stack length, l (mm)	200
Number of turns per HTS-excitation coil	150
Number of turns per armature coil	53
Slot fill factor	0.6
HTS wire material	Bi-2223
Iron material	DW360

set as 5000 At. In this case, the flux density in the air-gap is about 1.5 T and that in the mover tooth is up to 2.1 T. Moreover, the measured I/V characteristics of the fabricated HTS excitation coil is given in Fig. 10(b). It can be seen that the HTS excitation coil apparently lost its superconducting properties when the injected excitation current exceeds 40 A, which indicates the critical excitation current for the fabricated HTS excitation coil. Considering the number of turns per HTS-excitation coil, the HTS-excitation MMF can reach 6000 At while ensuring the superconducting characteristics of the HTS coil. And then, an optimized HTS-MFSL machine is finally determined, and its key design parameters are listed in Table 3.

IV. ELECTROMAGNETIC PERFORMANCE ANALYSIS

A. FLUX DENSITY AND NO-LOAD BACK-EMF

The no-load flux density distribution by 5000 At HTS-excitation and the corresponding air-gap flux density waveform along the longitude in the range of ten times τ_s are figured in the Fig. 11(a) and 11(b), respectively. It is obvious from Fig. 11(a) that the Phase C module is located at the position providing the maximum flux linkage for the Phase C armature windings, and thus the flux density of the mover teeth on the Phase C module reaches a high value around 1.9 T, which is also evidenced by the air-gap flux density up to 1.55 T as shown in Fig. 11(b). Moreover, it shows that the magnetic field between two adjacent phase modules almost has no interference on each other, which is helpful to achieve a reliable fault tolerant operation.

From what has been discussed above, the formula of the no-load back-EMF e_0 in the linear machine can be referred to as:

$$e_0 = \frac{d\psi_{\mathrm{HTS}}}{dt} = \frac{d\psi_{\mathrm{HTS}}}{dx}\frac{dx}{dt} = v\frac{d\psi_{\mathrm{HTS}}}{dx} \tag{4}$$

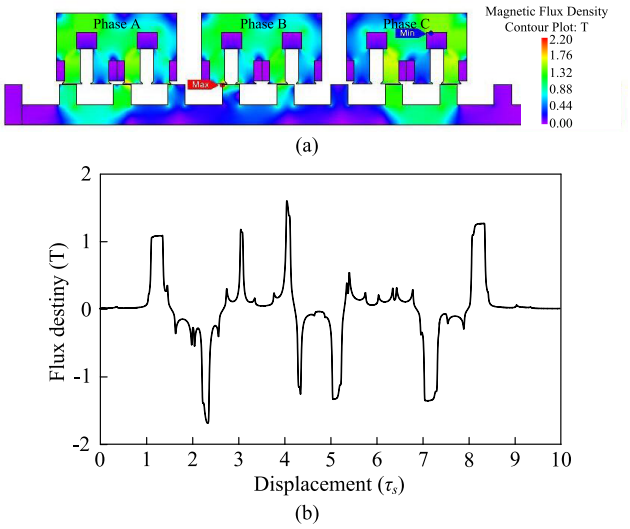

FIGURE 11. Flux destiny under no load condition. (a) Flux density distribution. (b) Air-gap flux density waveform along the longitude.

where ψ_{HTS} represents the winding flux linkage caused by the HTS-excitation, while x is the displacement of the mover, and v denotes the mover speed. By the means of 2D-FEM, the no-load back-EMF of Coil A1 and Coil A2 are calculated and described in Fig. 12(a). It can be seen that there is a phase angle difference of 180° electric degrees between them, which is consistent with the theoretical principle analysis.

And by connecting the Coil A1 and Coil A2 in reverse series, the back-EMF of the phase A under no load condition is also calculated, shown in Fig. 12(a). In addition, Fig. 12(b) gives the no-load back-EMF waveforms of the 3-phases, which shows that the longitudinal end-effect on the phase-EMF is decreased significantly with the design of phase modular mover. Besides, the harmonic analysis points out that the total harmonic distortion (THD) of the phase no-load back-EMF is only 7.6%. Hence, the brushless alternating current (BLAC) control is suitable for the designed machine. Moreover, Fig. 12(c) shows the phase no-load back-EMF waveforms of the proposed HTS-MFSL machine with different HTS-excitation MMF. It can be seen that with the increase of the HTS-excitation MMF, the no-load back-EMF also increases, but the growth rate of the no-load back-EMF amplitude gradually slows due to the non-linear influence of the iron magnetic saturation, which also matches with the HTS-excitation characteristic analysis as shown in Fig. 10(a). And it indicates that the phase back-EMF can be easily regulated by changing the HTS-excitation current to meet various control demands.

B. SELF-INDUCTANCE AND MUTUAL-INDUCTANCE

The physical configuration of the machine can determine the winding inductances. The self-inductances of Coil A1, Coil A2 and phase A without taking the magnetic saturation into consideration are displayed in Fig. 13(a), which means the rated current (namely, 45 A) is applied to the windings of the phase A while no current is applied to the HTS-excitation

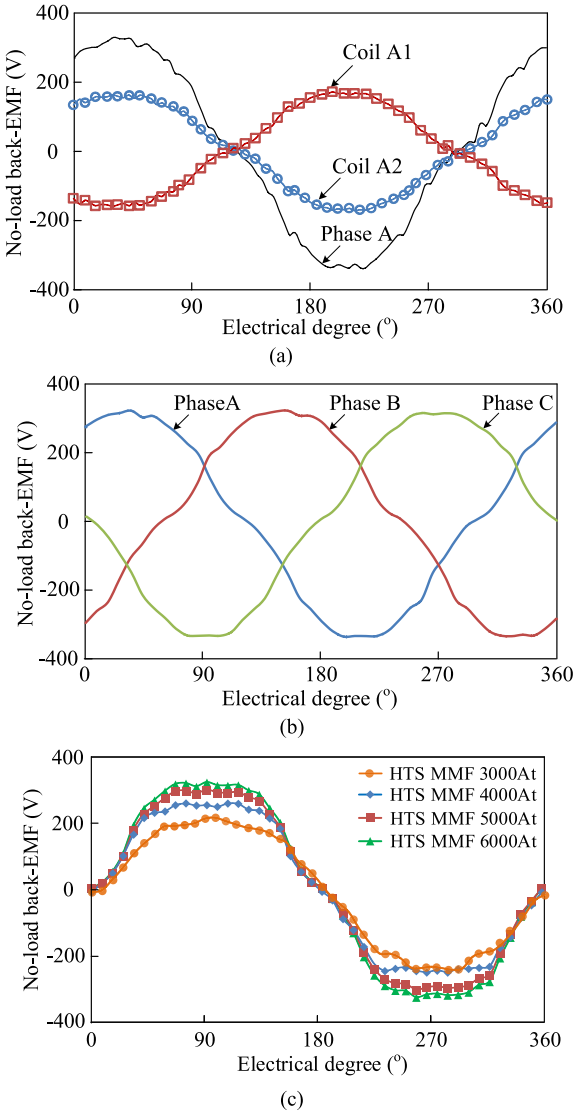

FIGURE 12. No-load back-EMF waveforms. (a) Coil A1, Coil A2 and phase A. (b) Three phases. (c) Under different HTS-excitation MMF.

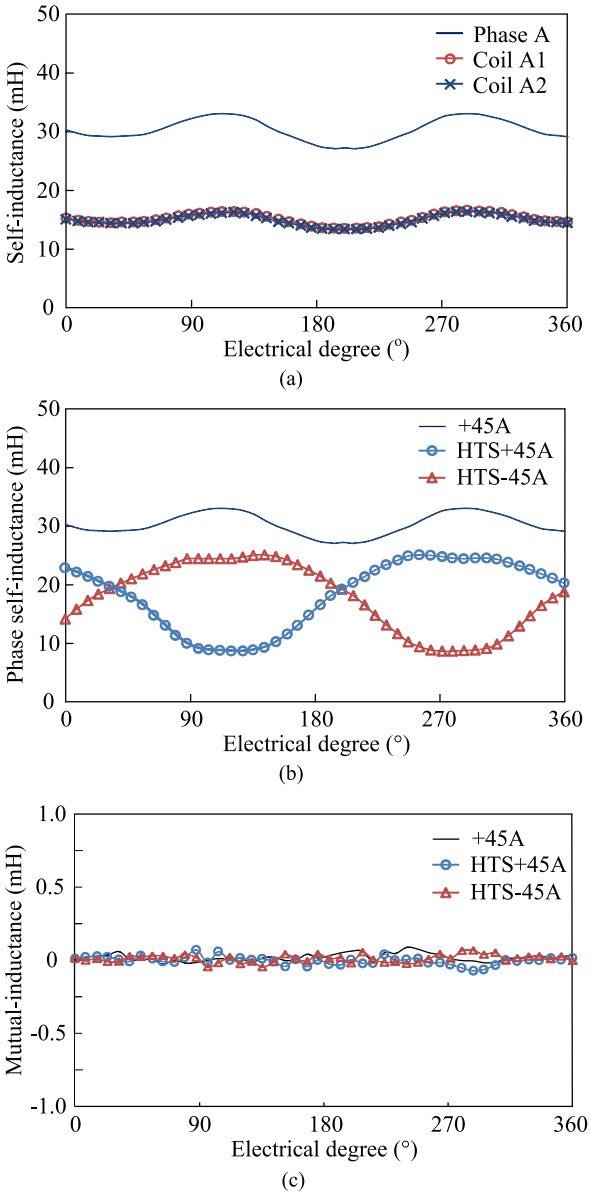

FIGURE 13. Inductance characteristics of the proposed HTS-MFSL machine under different field conditions. (a) Self-inductance when applying phase armature current 45 A with no HTS-excitation. (b) Phase self-inductance. (c) Phase mutual-inductance.

windings. It is obvious that there is little differences between the self-inductances of Coil A1 and Coil A2 due to the structural symmetry of each phase module, but the changing of the phase self-inductance with the different positions of the mover shows a little large fluctuation, which is caused by the double salient structure of each phase module.

To accurately calculate the inductance, the investigation into the self-inductance characteristics of the designed machine is completed by adopting the method of considering the magnetic saturation. The results are depicted in Fig. 13(b), where '+45 A', 'HTS + 45 A' and 'HTS − 45 A' indicate three different field conditions, which means only applying the rated phase armature current 45 A, applying the 5000 At HTS-excitation with rated phase current to strengthen the magnetic field (HTS + 45 A), or to weaken the magnetic field (HTS − 45 A), respectively. It is clear that the phase self-inductances when the phase armature current and HTS-excitation are both applied are much lower compared to that of only applying phase armature current because of the oversaturation of the magnetic circuit. Meanwhile, the average values and the shapes of the phase self-inductance under the condition of 'HTS+45 A' and 'HTS−45 A' are nearly the same, which indicates that the armature field has little effect on the strong HTS-excitation field in the designed machine. However, the fluctuation of the phase self-inductance when taking the HTS-excitation field into account is slightly larger than that without it due to the progressively severe magnetic flux leakage.

What's more, the advantageous feature of the phase modular mover design in the proposed machine is that each

phase module has its own separate magnetic circuit, which helps to prevent the effects of the fault phase imposing on the healthy phases under the fault condition, thus attaining a highly reliable operation. To some extent the mutual inductance as a critical parameter can refer to the magnetic coupling characteristics between phases. Therefore, the phase mutual-inductances of the machine are calculated under three different field conditions, and the results are shown in Fig. 13(c). It can be found that the phase mutual-inductances of the proposed HTS-MFSL machine are always very small, almost zero. Hence, the fault phase has minimum, even no impact upon the others, that is, the machine can still operate with other healthy phases working during loss of one phase. Therefore, it can be expected that the proposed machine will be a viable candidate of fault tolerant machine.

C. COGGING FORCE

It is known that when the HTS windings are applied with the excitation current with the armature windings open circuited, due to the tooth-slot alternation, there will be a cogging force on the mover, which can enlarge the thrust force pulsation. In order to obtain satisfactory thrust force performance, it is a valuable work to take measures to suppress the cogging force. With the help of the 2D-FEM, the cogging force varying with the mover movement in the designed machine can be obtained and compared as shown in Fig. 14. From Fig. 14(a) and 14(b), it indicates that the peak value of the cogging force of each phase module is pretty high, up to 640 N, but a 120° electric degrees shift between the cogging force of each phase module exists. Hence, the total cogging force which is attained by summing these three phase module cogging forces (denoted by 'Sum' in Fig. 14(b)) can be significantly weakened by 76%, to only 155 N, namely, there is a complementary effect which thanks to the phase modular mover design to greatly facilitate cogging force reduction. In addition, the cogging force on the overall mover ,which consists of three phase modules, known as 'FEM_whole', can also be directly calculated by applying the 2D-FEM, and in Fig. 14(c), it is depicted and compared with the 'Sum'. It shows that the 'FEM_whole' matches well with the 'Sum', which confirms the fact that the design of the modular mover can effectively offset the cogging force in the proposed HTS-MFSL machine.

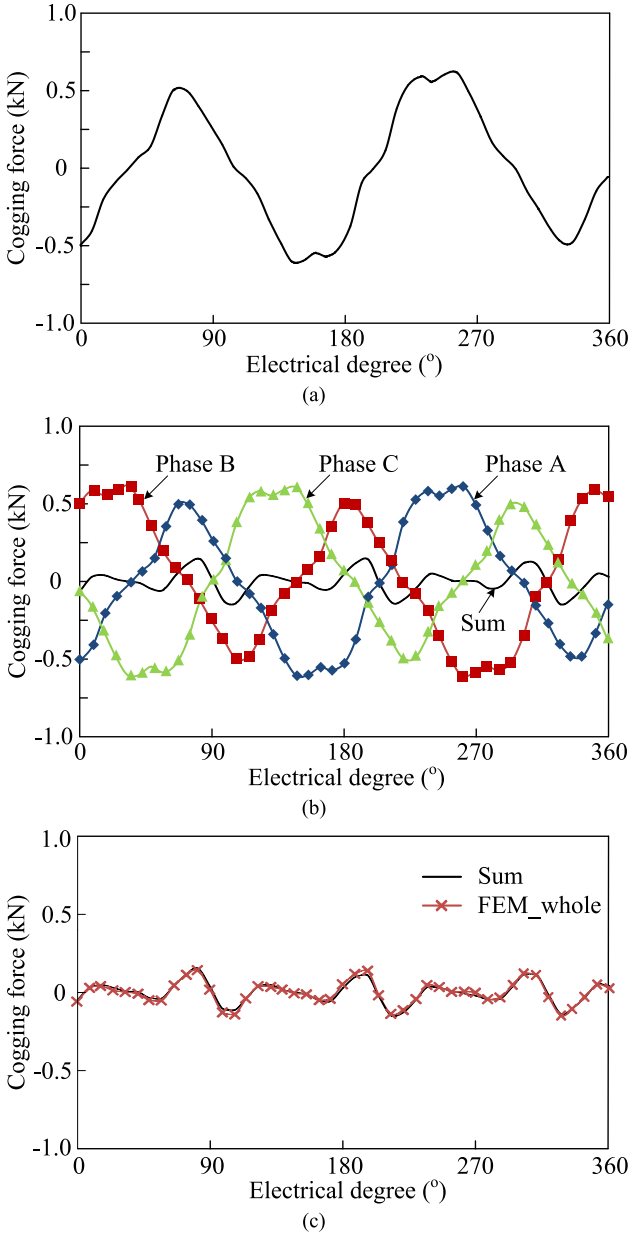

FIGURE 14. Cogging force analysis of the designed machine. (a) Phase A module. (b) Each phase module and the sum. (c) Comparison based on two calculation methods.

D. THRUST FORCE AND NORMAL FORCE

Considering the fact that the phase back-EMF of the designed machine is nearly sinusoidal, to evaluate its electromagnetic thrust force characteristics, the brushless AC (BLAC) operation can be applied. Generally, $i_d = 0$ control method is adopted to keep the armature current and the back-EMF in the same phase with each other. Then, with the help of the 2D-FEM, the thrust force of the designed machine is computed and depicted in Fig. 15(a), which shows that the maximum value, minimum value and average value of the thrust force are 3.72 kN, 3.45 kN and 3.61 kN, respectively. In addition, the thrust force ripple K_{e_rip} can be defined as

$$K_{e\_\mathrm{rip}} = \frac{F_{e\_\max} - F_{e\_\min}}{F_{e\_\mathrm{avg}}} \times 100\% \tag{5}$$

where F_{e_min}, F_{e_max} and F_{e_avg} are the minimum value, maximum value and average value of the thrust force, respectively. It can be seen that the calculated thrust force ripple accounts only about 7.5%, which is mainly caused by the cogging force. In addition, the electromagnetic thrust force

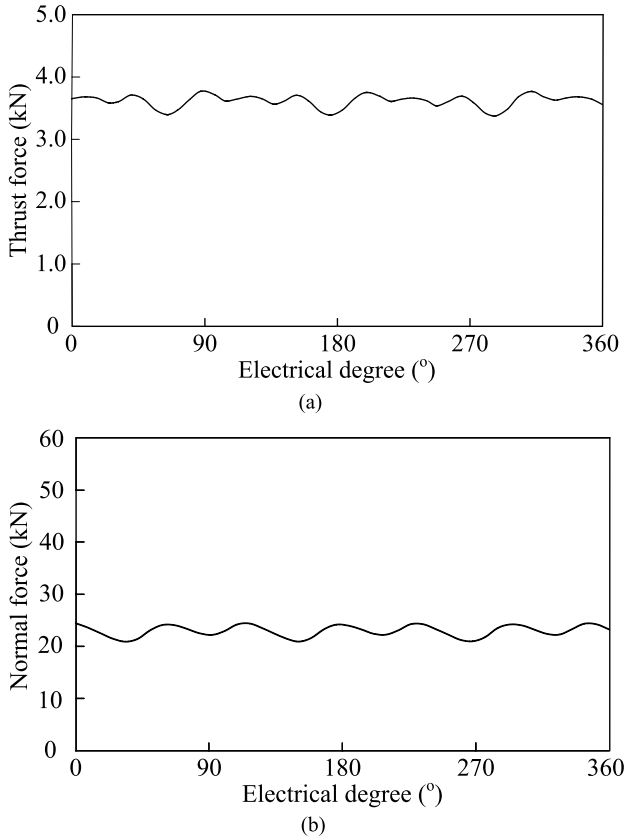

FIGURE 15. Force performance characteristics of the designed machine in the BLAC operation. (a) Thrust force. (b) Normal force.

can be computed by

$$F_{e\_\mathrm{cal}} = \sum_{k=a}^{c} \left(\frac{1}{2} i_k^2 \frac{dL_{kk}}{dx} + i_k \frac{d\psi_{\mathrm{HTS}k}}{dx} \right) \tag{6}$$

where k means each phase, namely, a, b, c, and i_k is the phase current, L_{kk} represents the phase self-inductance, $\psi_{\mathrm{HTS}k}$ denotes the phase flux linkage excited only by the HTS-excitation MMF, respectively. Thus, it can be obtained that the calculated thrust force F_{e_cal} is about 3.76 kN, which matches well with the FEM results. Apart from that, the normal force of the machine in the BLAC operation is also studied and shown in Fig. 15(b), which indicates that the value of the normal force is pretty high due to the adoption of the single-side structure.

V. CONCLUSION

In the paper, a novel HTS-MFSL machine designed for long-stator applications has been presented and analyzed. The proposed machine possesses a simple stator consisting of only iron to offer the reduced cost and high robustness, meanwhile it employs the attractive HTS excitation with static seals to easily obtain simple refrigeration system. Also, the phase modular mover structure is designed, which can greatly offset the cogging force, thus effectively reduce force ripple. Also, the modular mover pattern makes a good candidate for high fault tolerance due to independent phase magnetic circuits. With the help of the 2D-FEM, the electromagnetic performance analysis of the proposed machine is conducted to verify its validity. The results confirm that the 3-phase symmetrical and sinusoidal back-EMF can be offered, and the almost zero mutual-inductance between adjacent phases indicate a good phase magnetic circuit independence, while the small force ripple is achieved due to greatly reduced cogging force.

REFERENCES

[1] R. Hellinger and P. Mnich, "Linear motor-powered transportation: History, present status, and future outlook," *Proc. IEEE*, vol. 97, no. 11, pp. 1892–1900, Nov. 2009.

[2] K. Suzuki, Y. J. Kim, and H. Dohmeki, "Driving method of permanent-magnet linear synchronous motor with the stationary discontinuous armature for long-distance transportation system," *IEEE Trans. Ind. Electron.*, vol. 59, no. 5, pp. 2227–2235, May 2012.

[3] G. Stumberger, D. Zarko, M. T. Aydemir, and T. A. Lipo, "Design and comparison of linear synchronous motor and linear induction motor for electromagnetic aircraft launch system," in *Proc. IEMDC*, Jun. 2003, pp. 494–500.

[4] R. Cao *et al.*, "Modeling of a complementary and modular linear flux-switching permanent magnet motor for urban rail transit applications," *IEEE Trans. Energy Convers.*, vol. 27, no. 2, pp. 489–497, Jun. 2012.

[5] R. Cao, M. Cheng, C. Mi, W. Hua, and W. Zhao, "Comparison of complementary and modular linear flux-switching motors with different mover and stator pole pitch," *IEEE Trans. Magn.*, vol. 49, no. 4, pp. 1493–1504, Apr. 2013.

[6] R. Cao, M. Cheng, C. Mi, W. Hua, and W. Zhao, "A linear doubly salient permanent-magnet motor with modular and complementary structure," *IEEE Trans. Magn.*, vol. 47, no. 12, pp. 4809–4821, Dec. 2011.

[7] W. Zhao, J. Ji, G. Liu, Y. Du, and M. Cheng, "Design and analysis of a new modular linear flux-reversal permanent-magnet motor," *IEEE Trans. Appl. Supercond.*, vol. 24, no. 3, Jun. 2014, Art no. 5200305.

[8] R. Cao, M. Cheng, C. Mi, and W. Hua, "Influence of leading design parameters on the force performance of a complementary and modular linear flux-switching permanent-magnet motor," *IEEE Trans. Ind. Electron.*, vol. 61, no. 5, pp. 2165–2175, May 2014.

[9] R. Qu, Y. Liu, and J. Wang, "Review of superconducting generator topologies for direct-drive wind turbines," *IEEE Trans. Appl. Supercond.*, vol. 23, no. 3, Jun. 2013, Art no. 5201108.

[10] L. Zheng, J. Jin, Y. Guo, W. Xu, and J. Zhu, "Performance analysis of an HTS magnetic suspension and propulsion system with a double-sided HTS linear synchronous motor," *IEEE Trans. Magn.*, vol. 48, no. 2, pp. 655–658, Feb. 2012.

[11] Y. B. Wang, M. Chen, T. W. Ching, and K. T. Chau, "Design and analysis of a new HTS axial-field flux-switching machine," *IEEE Trans. Appl. Supercond.*, vol. 25, no. 3, Jun. 2015, Art no. 5200905.

[12] X. Li, S. Liu, and Y. Wang, "Design and analysis of a stator HTS field-modulated machine for direct-drive applications," *IEEE Trans. Appl. Supercond.*, vol. 27, no. 4, Jun. 2017, Art no. 5201005.

[13] Y. Wang, J. Sun, Z. Zou, Z. Wang, and K. T. Chau, "Design and analysis of a HTS flux-switching machine for wind energy conversion," *IEEE Trans. Appl. Supercond.*, vol. 23, no. 3, Jun. 2013, Art no. 5000904.

[14] W. Li, K. T. Chau, C. Liu, and C. Qiu, "Design and analysis of a flux-controllable linear variable reluctance machine," *IEEE Trans. Appl. Supercond.*, vol. 24, no. 3, Art no. 5200604, Jun. 2014.

[15] F. Xiao, Y. Du, Y. Wang, M. Chen, T. W. Ching, and X. Liu, "Modeling and analysis of a linear stator permanent-magnet Vernier HTS machine," *IEEE Trans. Appl. Supercond.*, vol. 25, no. 3, Jun. 2015, Art no. 5202104.

[16] C. Liu, K. T. Chau, J. Zhong, and J. Li, "Design and analysis of a HTS brushless doubly-fed doubly-salient machine," *IEEE Trans. Appl. Supercond.*, vol. 21, no. 3, pp. 1119–1122, Jun. 2011.

[17] Y. Liu, S. Niu, S. L. Ho, W. N. Fu, and T. W. Ching, "Design and analysis of a new HTS double-stator doubly fed wind generator," *IEEE Trans. Appl. Supercond.*, vol. 25, no. 3, Jun. 2015, Art no. 5200804.

[18] J. Rao and W. Xu, "Modular stator high temperature superconducting flux-switching machines," *IEEE Trans. Appl. Supercond.*, vol. 24, no. 5, Oct. 2014, Art no. 0601405.
[19] X. Zhu, D. Fan, L. Mo, Y. Chen, and L. Quan, "Multiobjective optimization design of a double-rotor flux-switching permanent magnet machine considering multimode operation," *IEEE Trans. Ind. Electron.*, vol. 66, no. 1, pp. 641–653, Jan. 2019.
[20] X. Zhu, Z. Xiang, L. Quan, W. Wu, and Y. Du, "Multimode optimization design methodology for a flux-controllable stator permanent magnet memory motor considering driving cycles," *IEEE Trans. Ind. Electron.*, vol. 65, no. 7, pp. 5353–5366, Jul. 2018.

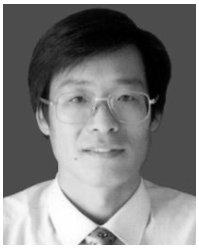

WENZHONG MA was born in Shandong, China. He received the B.S. and M.S.E. degrees in electrical engineering from the Harbin Institute of Technology, Harbin, China, in 1993 and 1995, respectively, and the Ph.D. degree in electrical engineering from the Institute of Electrical Engineering, Chinese Academy of Sciences, Beijing, China, in 2006.

Since 1995, he has been a Faculty Member with the China University of Petroleum (East China), Qingdao, China, where he is currently a Professor with the Department of Electrical Engineering. From 2002 to 2006, he was involved in a national key project for Shanghai high-speed maglev train systems, which is the first commercial high-speed maglev train. He was a Visiting Professor with the University of Alberta, Edmonton, AB, Canada, from 2013 to 2014. He has taught a wide range of courses about electric machinery and power electronics, including electric machinery and drive systems, ac variable speed systems, power electronics, electric circuit analysis, and electrical energy saving systems. He has done extensive research in electrical engineering and automation, including power electronic systems, converters, renewable energy, distributed micro grid, HVDC, motor design, and motor drives. He took charge of the commissioning and testing work of the long stator line motor, propulsion systems, and power distribution systems. He has fulfilled the optimization of the long stator line motor systems which is part of the Key Projects of the National High Technology Research and Development Program of China (863 Program). He has authored six books and authored or co-authored more than 30 technical papers. He holds six patents in his areas of interest.

Dr. Ma is a Committee Member of the China Electrotechnical Society.

XIAOYANG WANG was born in Shandong, China. He received the B.Sc. degree in electrical engineering and automation from the College of Electrical and Electronic Engineering, Shandong University of Technology, Zibo, China, in 2016. He is currently pursuing the M.Sc. degree in electrical engineering with the China University of Petroleum (East China).

His research interests include the design and analysis of modular flux-switching linear machine, and switched reluctance linear machine.

YUBIN WANG was born in Shandong, China. He received the M.Sc. degree in control theory and control engineering from the College of Electrical Engineering and Automation, Shandong University of Science and Technology, Jinan, China, in 2003, and the Ph.D. degree in electrical engineering from the Department of Electrical Engineering, Southeast University, Nanjing, China, in 2011.

Since 2003, he has been with the China University of Petroleum (East China), Qingdao, China, where he is currently an Associate Professor with the College of Information and Control Engineering. In 2013, he was a Research Assistant with the Department of Electrical and Electronic Engineering, The University of Hong Kong. He has authored or co-authored more than 30 technical papers. He holds ten patents in his areas of interest. His teaching and research interest includes electromagnetic design and analysis of high-temperature superconducting generators with stationary seal and permanent magnet machines.

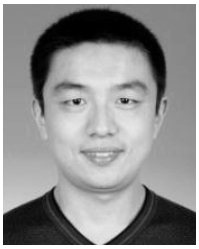

XIANGLIN LI was born in Shandong, China. He received the B.Sc. and M.Sc. degrees from the College of Information and Control Engineering, China University of Petroleum (East China), Qingdao, China, in 2007 and 2010, respectively, and the Ph.D. degree in electrical engineering from the School of Electrical Engineering, Southeast University, Nanjing, China, in 2015.

He was a Visiting Student with the Wisconsin Electric Machine and Power Electronics Consortium, University of Wisconsin–Madison, Madison, WI, USA, from 2012 to 2013, and a Research Assistant with the Department of Electrical and Electronic Engineering, The University of Hong Kong, Hong Kong, from 2014 to 2015. Since 2015, he has been with the China University of Petroleum (East China), where he is currently an Associate Professor with the College of Information and Control Engineering. He has authored or co-authored more than 20 technical papers. He holds five patents in his areas of interest. His teaching and research interests include magnetic gear, design and analysis of permanent-magnet machines, and high-temperature superconducting machines with stationary seal.